Conformation and mechanical properties of closed diblock fibers

Sumanth Swaminathan, Francisco J. Solis, and Monica Olvera de la Cruz

Phys. Rev. E **83**, 061912 — Published 15 June 2011

DOI: 10.1103/PhysRevE.83.061912

Conformation and mechanical properties of closed diblock fibers

Sumanth Swaminathan,[1] Francisco J. Solis,[1,2] and Monica Olvera de la Cruz[1]

[1] *Department of Materials Science and Engineering, Northwestern University, Evanston, Illinois 60208-3108*

[2] *Division of Mathematical and Natural Sciences, Arizona State University, Glendale, AZ, 85069*

We analyze the conformations and mechanical properties of closed diblock fibers. In our model, the length fraction of each component and the total fiber length are controlled by tunable chemical potentials. Our formalism can describe fibers in which one block is a bare polymer while the other is an adsorbed protein-filament complex; these blocks maintain different bending rigidities and spontaneous curvatures. We analytically calculate the shape of two-component polymers for all values of the material parameters and chemical potentials. Our results yield: a complete analytical description of all possible two-component polymer conformations, a phase portrait detailing the parameter spaces in which these shapes occur, and the identification of spontaneous transitions between shapes driven by environmental changes.

PACS numbers: 82.45.Gj, 61.20.Qg, 64.70.Ja, 68.03.Cd

INTRODUCTION

Many biological filaments exhibit complex conformation transformations upon adsorption of proteins. DNA looping can occur, for example, when proteins bind, aggregate, and subsequently induce bending and twisting. Protein adsorption further promotes changes in the effective mechanical properties of the DNA molecule [1] and its conformation [2, 3]. Other biological polymers including actin, microtubules, and general cytoskeletal filaments exhibit similar behavior in addition to self-assembling processes upon interaction with crosslinking and motor proteins [4–6]. Transformations in many biofilaments play an integral role in biological activity. Loops in DNA, for example, affect downstream functions, such as protein-DNA assembly during replication, recombination, and condensation [7]. ***It has been further suggested that nucleosome repositioning on short DNA segments is mediated by DNA looping [8].***

The intricate relationship between chemical interactions and associated mechanical transformations in biofilaments is yet to be fully explored. The diversity of naturally occurring molecular complexes calls for a systematic analysis of the underlying mechanisms governing conformation transformations. Resolution of these mechanisms could yield opportunities to develop new types of environmentally responsive molecular systems.

In this work we study the properties of closed, heterogeneous, two-component polymers. The mechanics of linear polymers and fibers has been studied extensively with a variety of theoretical formalisms [9–16]. To date, however, a comprehensive analytical treatment of multicomponent polymers is yet to be adequately completed. We consider a model in which each polymer is comprised of a single flexible diblock. For example, one block may consist of a bare polymer while the second is rich in adsorbed proteins. Since adsorbed molecules can change the effective length of a polymer, we consider a formalism in which the relative lengths are not fixed but rather controlled by tunable chemical potentials.

Our model specifically focuses on planar structures. The framework and results presented in this paper are directly useful for describing many systems physically confined to surfaces such as those examined by electron or atomic force microscopy [17]. DNA-protein interactions, in particular, are frequently studied on surfaces [18]; characterization of DNA often requires its adsorption onto surfaces in the presence of proteins' multivalent ions [19].

Closed structures with nonuniform bending rigidity arise in a variety of systems [20]. One biological example in which structural heterogeneities affect functionality is the marginal band in thrombocytes; in addition to providing structural support to the cell membrane and resistance to capillary flow stresses [21], the marginal band has a nonuniform spontaneous curvature which is believed to form an important basis for the flattened, ellipsoidal shape of cells [22].

Our methodology is adaptable to three dimensional systems with many components. The analysis in this paper employs the language of quadratic constraints previously developed for shapes of membranes [23, 24]. Our end result is a complete description of planar, two-component polymer conformations for all possible material parameters.

We begin by constructing a free energy F_p for each component $p = a, b$. In each block, the energy is the integral of a density, $\mathcal{F}_p$;

$$F_p = \int_{L_p} ds \mathcal{F}_p = \int_{L_p} ds \left[\frac{1}{2} \Lambda_s (\kappa - C_p)^2 - \mu_p \right] - G, \quad (1)$$

where Λ is the bending rigidity, κ the curvature, C the spontaneous curvature, and s the arc length. For brevity, we omit the subscript p where possible. The first term in the integral corresponds to the bending energy. In the

second term, the chemical potential μ acts as a Lagrange multiplier to fix the length of component p. Finally, G is a constraint required to express the free energy in terms of the Frenet-Serret vectors $(\mathbf{t}, \mathbf{n}, \mathbf{b})$. G is written explicitly as,

$$\begin{aligned} G = \int dt\sqrt{g}\,[-\mathbf{f}\cdot(\mathbf{t}-\mathbf{r}') - \alpha_{nn}(\mathbf{n}\cdot\mathbf{n}-1) \\ - \alpha_{tt}(\mathbf{t}\cdot\mathbf{t}-1) - \alpha_{tn}\mathbf{t}\cdot\mathbf{n} - \alpha_{ttn}(\mathbf{t}'\times\mathbf{n})\cdot\mathbf{t}]\,. \end{aligned} \tag{2}$$

In the above expression, the shape parameter t is related to the arc length s through the metric factor $\sqrt{g} = ds/dt$. Primes denote derivatives with respect to arc-length; these are constructed for a generic function h as $h' = (\sqrt{g})^{-1}(dh/dt)$. The Lagrange multiplier $\mathbf{f}$ defines the tangent vector $\mathbf{t}$ in terms of the parameterized path $\mathbf{r}$ and can be identified as the cohesive force in the fiber. The remaining constraints have associated Lagrange multipliers α_{nn}, α_{tt}, α_{tn}, α_{nn}.

Variations with respect to $\mathbf{t}$, $\mathbf{n}$, $\mathbf{f}$, $\mathbf{r}$ and $\sqrt{g}$ lead to the system of Euler-Lagrange equations governing the polymer's conformation, the conserved quantities, and the boundary conditions at the junction of the two components. The equations that arise from a variation with respect to $\mathbf{t}$ and $\mathbf{r}$ explicitly yield an expression for the force and force conservation respectively:

$$\mathbf{f} = -\Lambda\frac{d}{ds}[\mathbf{t}' - C\mathbf{n}] - 2\alpha_{tt}\mathbf{t} - \alpha_{tn}\mathbf{n} - \alpha_{ttn}\mathbf{t}'\times\mathbf{n} \tag{3}$$

$$\mathbf{f}' = \mathbf{0}. \tag{4}$$

We assume, without loss of generality, that the force points in the $\mathbf{x}$-direction. Invariance of the functional with respect to rotations in space leads to a set of relations for the torque τ. Only the z-component τ_z is nonzero and satisfies,

$$\tau_z = \Lambda(\kappa - C)\mathbf{b}\cdot\mathbf{k} + (\mathbf{r}\times\mathbf{f})\cdot\mathbf{k} \tag{5}$$

$$\tau_z{}' = 0. \tag{6}$$

As we consider only planar shapes, the angle defined by the relative orientation of $\mathbf{t}$ and $\mathbf{f}$, $\mathbf{f}\cdot\mathbf{t} = f\cos\theta$, is a useful coordinate for analysis. The curvature is a positive quantity that can be written as $\kappa = w\theta'$, where $w = sgn(\theta') = (\mathbf{t}\times\mathbf{n})\cdot\mathbf{k}$ is the sign of the curvature.

Using the variable θ, equation (3) can be transformed to,

$$-\Lambda\theta'' + f\sin\theta = 0. \tag{7}$$

The equation resulting from the variation with respect to the metric factor turns out to be an integral of Eq. (7):

$$-\frac{1}{2}\Lambda\theta'^2 + \frac{1}{2}\Lambda C^2 - f\cos\theta - \mu = 0. \tag{8}$$

Upon introduction of the intrinsic component of the torque $\tau^i = \Lambda(\theta' - wC)$, we can write,

$$-\frac{1}{2\Lambda}\left(\tau^i\right)^2 - w\tau^i C - f\cos\theta - \mu = 0. \tag{9}$$

At this point, we note the first of many conditions on the parameters and variables that are required for the existence of solutions. As the square of the curvature is positive, we must have:

$$D = \frac{\Lambda}{2}C^2 - \mu \geq f\cos\theta. \tag{10}$$

The parameter D will be indexed as D_a or D_b according to the region to which it corresponds.

The variational analysis of the two components leads to boundary terms; demanding that these combined terms vanish gives rise to boundary conditions between segments. At the boundary, the following conditions apply to the tangent vector, force, and intrinsic torque component:

$$\begin{aligned} \mathbf{t}_a &= \mathbf{t}_b, \\ \mathbf{f}_a &= \mathbf{f}_b, \\ \tau_a^i &= \tau_b^i. \end{aligned} \tag{11}$$

The continuity of the tangent vector implies that the two segments make contact at an angle θ_c. We denote the intrinsic torque value at the junction by τ_c. Substituting Eq. (11) into Eq. (9) for each component yields after algebraic manipulations:

$$\begin{aligned} \left(\frac{1}{\Lambda_a} + \frac{1}{\Lambda_b}\right)\tau_c^2 + 2(w_aC_a + w_bC_b)\tau_c \\ + 4f\cos\theta_c + 2(\mu_b + \mu_a) = 0. \end{aligned} \tag{12}$$

$$\begin{aligned} \left(\frac{1}{\Lambda_b} - \frac{1}{\Lambda_a}\right)\tau_c^2 + 2(w_bC_b - w_aC_a)\tau_c \\ + 2\left(\mu_b - \mu_a\right) = 0. \end{aligned} \tag{13}$$

We therefore see that that the intrinsic torque at contact can be determined from the material parameters Λ and C, and the difference in the chemical potentials $\Delta\mu = \mu_b - \mu_a$. Solutions exist when the following holds:

$$(w_bC_b - w_aC_a)^2 - 2\Delta\mu(\frac{1}{\Lambda_b} - \frac{1}{\Lambda_a}) \leq 0 \tag{14}$$

The resulting value of the intrinsic torque defines a unique value for the combination $f\cos\theta_c + \bar{\mu}$ where $\bar{\mu} = \frac{1}{2}(\mu_b + \mu_a)$. One can see from the definition of the internal torque that $w\tau_c + \Lambda C \geq 0$; this condition in addition to (10) and (14), helps narrow the range of material parameters that yield solutions.

The explicit construction of the fiber shapes is simplest when parameterized by the angle θ. We integrate our equations to obtain:

$$\mathbf{r_2} - \mathbf{r_1} = A\int_{\theta_1}^{\theta_2} w\,d\theta\frac{\mathbf{t}}{\sqrt{\chi - q\cos\theta}}, \tag{15}$$

in each component. Here we use the orientation of the curvature w and $\chi = sgn(D)$. The amplitude of the trajectory is given by $A = \Lambda/(2|D|)^{1/2}$ and the extension

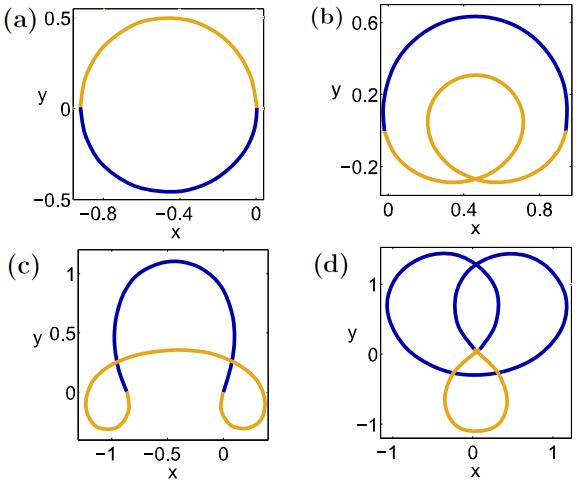

FIG. 1. (Color online) Sample equilibrium conformations showing a (a) ring structure, (b) single-loop structure (c) single-loop structure in which the two components have opposite curvature (d) double loop structure. The parameters used in each case were: (a) $\Lambda_a/\Lambda_b = 0.5$, $C_a/C_b = 0.5$, $\Delta\mu = -0.27$, $\bar{\mu} = -0.55$, (b) $\Lambda_a/\Lambda_b = 0.5$, $C_a/C_b = 5$, $\Delta\mu = 3.29$, $\bar{\mu} = -3.92$, (c) $\Lambda_a/\Lambda_b = 5$, $C_a/C_b = 5$, $\Delta\mu = -1.40$, $\bar{\mu} = -0.82$, (d) $\Lambda_a/\Lambda_b = 5$, $C_a/C_b = 5$, $\Delta\mu = -0.087$, $\bar{\mu} = -0.28$.

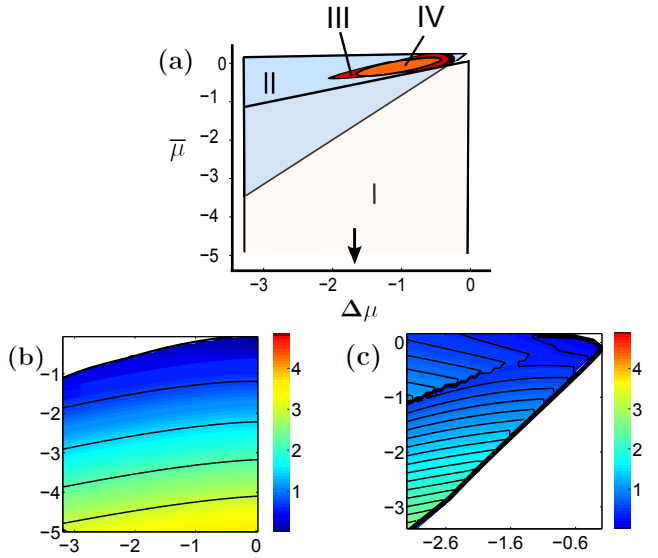

FIG. 2. (Color online) Phase portraits showing different types of solution topologies in the $(\Delta\mu\,,\,\bar{\mu})$ plane for the material parameters, $\Lambda_a/\Lambda_b = 5$, $C_a/C_b = 5$. In (a), region I corresponds to ring structures, II to single loop structures, III to double-loop structures, and IV to higher loop structures; the arrow indicates that region I extends infinitely in the $-\bar{\mu}$ direction. Figures (b) and (c) show energy per length contours overlaying the solution space corresponding to (b) ring structures and (c) single loop structures; these plots show that when topological regions overlap, the structures with fewer loops are energetically favorable.

parameter is $q = f/|D|$. The integrals can be explicitly expressed in terms of elliptic functions (not shown here for brevity). Integrations are only possible in regions where $\chi - q\cos\theta \geq 0$. If $\chi > 0$ and $q < 1$, the restriction is always satisfied. In all other cases, the region of integration is limited to values of the angle that lie on a region centered at $\theta = \pi$.

The previous results show that for a pair of segments exerting a given force on each other, the cosine of their contact angle is uniquely determined. The contact can then occur at angles $\pm\theta_c + 2\pi m$, with m an integer and θ_c restricted to the interval from 0 to π. The necessary condition for closure of the shapes is $\Delta\mathbf{r} = 0$. One can find closed configurations for a given set of parameters by first establishing a range of possible internal force values; this range is determined from the previous discussed set of conditions. Next, one can check whether the closure condition is satisfied for values in that range. The entire space of parameters can be systematically explored with this procedure.

The space of material parameters to explore can be reduced by suitable changes of energy and length scales. In particular, we can set $\Lambda_a = 1$ and $C_a = 1$ and vary the remaining material parameters (if $C_a = 0$, we can set $C_b = 1$ or $C_b = 0$). For each of these points in the parameter space, it is possible that multiple solutions will arise. The key characteristics of different types of solutions include the relative sign w and the number of loops exhibited by each species.

Fig. 1 shows sample equilibrium configurations of ring, single loop, and double loop structures. In each figure, the blue (lighter) segment identifies the component with the smaller bending rigidity. The examples shown in the figure demonstrate the large variety of conformations generated from our relatively simple model. It should be noted, however, that shapes (b)-(d) do not correspond to global minima for their respective parameter values. With a limited number of base parameters, tunable in physically meaningful ways, we recover conformations that appear in concrete settings: shapes (a)-(c) are similar to those found in the DNA-LacI complex [9]. The looped structure in (d) is similar to those found in *in vitro* experiments on induced knotting in DNA by means of SMC (structure maintenance of chromosome) proteins [26].

Fig. 2 shows a sample phase portrait in the chemical potential variables $\bar{\mu}$ and $\Delta\mu$. These variables determine in an implicit and non-linear way the lengths of the components. It is of course possible to invert this relation to determine the chemical potentials required to prescribe total and relative block length. Fig. 2 also shows contour plots of energy per length for different classes of solutions. Panels (b) and (c) clearly indicate that configurations with fewer loops are energetically favorable.

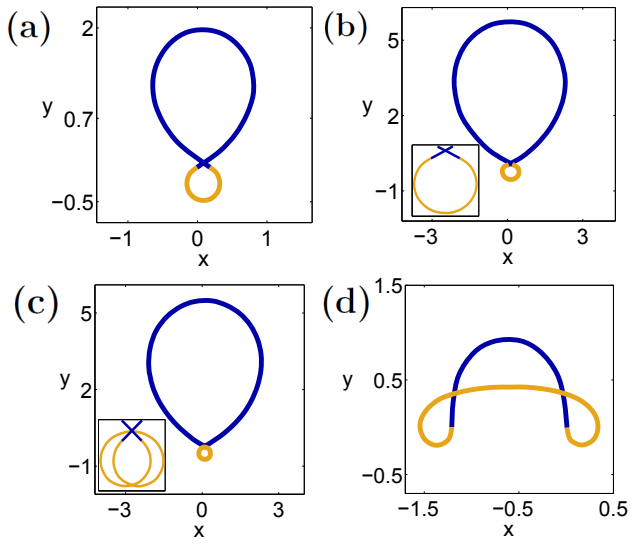

FIG. 3. (Color online) A topological transition induced by changes in chemical potentials. The parameters in all pictures are: $\Lambda_a = 1$,$\Lambda_b = 0.2$,$C_a = 1$,$C_b = 0.2$, and $\bar{\mu} = -0.75$. The individual snapshots correspond to (a) $\Delta\mu = -2.22$, (b)$\Delta\mu = -2.365$, (c) $\Delta\mu = -2.375$, and (d) $\Delta\mu = -2.52$. For clarity, the insets in (b) and (c) show magnifications of the minority component. We note that near the threshold dividing the two topological regions, the (b) single loop and (c) double loop structures retains similar majority component shapes.

Panel (a) reveals, however, that there are regions in the parameter space in which only looped structures exist. Hence, global minimum energy structures are not always ring-like.

Several important features of the phase diagram are worth emphasizing. First, we find that the regions in which multiple loop solutions are possible are generally nested inside a region of identical topology and fewer loops (but more than one loop). The higher looped structures may yet be relevant as transient states during dynamic shape transformations.

Next, we note that the boundaries of regions with specific topologies are characterized by $\mathbf{f} = 0$ and $D = 0$ for one of the components. These conditions physically correspond to the elongation of one component relative to the other. Small perturbation to physical parameters near these boundaries result in the selection of different topologies. One such example is depicted in Fig. 3.

Our model can be generalized and extended to incorporate further important details. For example, our model is planar and restricted to two dimensions. Similar analysis can be done in three dimensions where more complicated structures are possible. Furthermore, we have not considered the complications that arise from the friction with the substrate and the forces induced by self contact. Despite these limitations, our analysis has generated interesting results; we have identified a large number of possible shapes and the parametric conditions under which they occur. We have found conformations that mimic known structures, and we have identified interesting transitions driven by the tuning of system parameters. We have developed a robust formalism capable of describing a great variety of physically relevant structures.

This material is based upon work supported as part of the Non-Equilibrium Energy Research Center (NERC), an Energy Frontier Research Center funded by the U.S. Department of Energy, Office of Science, Office of Basic Energy Sciences under award number DE-SC0000989. F.S. acknowledges funding from the National Science Foundation under award number DMR-0805330.

[1] H. Zhang, J. F. Marko, Phys. Rev. E,**77**, 031916 (2008).
[2] E. Raspaud, M. Olvera de la Cruz, J. L. Sikorav, F. Livolant, Biophysical Journal **74**, 381 (1998).
[3] B. Xiao, R. C. Johnson, J. F. Marko, Nucleic Acids Res. (2010).
[4] L.C. Kapitein, E.J.G. Peterman, B.H. Kwok, J.H. Kim, T.M. Kapoor, C.F. Schmidt, Letters to Nature **435**, 114 (2005).
[5] B. R. McCullough, L. Blanchoin, J-L Martiel, E. M. de la Cruz, J. Mol. Biol **381,3**, 550 (2008).
[6] S. Swaminathan, F. Ziebert, I.S. Aranson, D. Karpeev Europhysics Letters, **90**, 28001, (2010).
[7] H. Echols, J. Biol Chem., **265**, 14697 (1990).
[8] I. M. Kulic, H. Schiessel, Biophys J., **84**, 3197, (2003).
[9] T. D. Lillian, S. Goyal, J. d. Kahn, E. Meyhofer, N. C. Perkins, Biophysical Journal, **95**, 5832, (2008).
[10] R. D. Kamien, T. C. Lubensky, P. Nelson, C. S. O'hern, Europhys Lett., **38**, 237 (1997).
[11] R. d. Kamien, Rev. of Mod. Phys., **88**,953 (2002).
[12] Y. Shi, J. E. Hearst, J. chem. Phys., **101,6**, 5186 (1994).
[13] G. Arreaga, R. Capovilla, C. Chryssomalakos, J. Guven, Phys. Rev. E., **65,3**, 031801 (2002).
[14] S. M. Klimenko, T. I. Tikkchonenko, V. M. Andreev, J. Mol. Biol., **23**, 523 (1967).
[15] J. F. Marko, E. D. Siggia, Macromolecules., **27**,981 (2002).
[16] Z. Haijun, Z. Yang, O.Y. Zhong-Can., Phys. Rev. Lett., **82**,4560 (1999).
[17] H. G. Hansma, Ann. Rev. Phys. Chem., **52**, 71 (2001).
[18] C. Bustamante, C. Rivetti, Annu. Rev. Biophys. Biomol. Struct., **25**, 395 (1996).
[19] H. Cheng, K. Zhang, M. Olvera de la Cruz, M. J. Bedzyk, Biophysical Journal., **90**, 1164 (2006).
[20] E. Katifori, S. Alben, D. R. Nelson, Phys. Rev. E., **79**, 056604 (2009).
[21] J. J-Silverstein, W. Cohen, J. Cell Biol., **98**, 2118 (1984).
[22] W. D. Cohen, Y. Sorokina, I. Sanchez, Cell Motil. Cytoskeleton., **40**, 238, (1998).
[23] J. Guven, Journal of Physics A., **37,28**, L313, (2004).
[24] F. J. Solis, C. M. Funkhouser, K. Thornton, Europhy. Lett., **82,3**, 38001 (2008).
[25] J. A. Libera, H. Cheng, M. Olvera de la Cruz, M. J. Bedzyk, J. Phys. Chem. B., **109**, 23001 (2005).
[26] J. E. Stray, N. J. Crisona, B. P. Belotserkovskii, J. E. Lindsley, N. R. Cozzarelli, J. Biol Chem., **280,41**, (2005).